Effects of titanium substitutions for aluminum and tungsten in Co-10Ni-9Al-9W (at%) superalloys

Peter J. Bocchini[a,*], Chantal K. Sudbrack[b], Ronald D. Noebe[b], David C. Dunand[a,d], David N. Seidman[a,c,d]

[a] Department of Materials Science and Engineering, Northwestern University, 2220 Campus Drive, Evanston, IL 60208-3108, USA
[b] NASA Glenn Research Center, 21000 Brookpark Road, Cleveland, OH 44135, USA
[c] Northwestern University Center for Atom-Probe Tomography (NUCAPT), 2220 Campus Drive, Evanston, IL 60208-3108, USA
[d] NanoAl LLC, Illinois Science + Technology Park, 8025 Lamon Ave, Suite 446, Skokie, IL 60077, USA

ARTICLE INFO

ABSTRACT

Polycrystalline Co-10Ni-(9 – x)Al-(9 – x)W-2xTi at% (x = 0, 1, 2, 3, 4) alloys with γ(f.c.c.) plus γ'(L1$_2$) microstructures are investigated, where the γ'(L1$_2$)-formers Al and W are replaced with Ti. Upon aging, the initially cuboidal γ'(L1$_2$)-precipitates grow and develop a rounded morphology. After 256 h of aging at 1000 °C, the precipitates in the 6 and 8 at% Ti alloys coalesce and develop an irregular, elongated morphology. After 1000 h of aging, replacement of W and Al with Ti increases both the mean radius, $< R >$, and volume fraction, ϕ, of the γ'(L1$_2$)-phase from $< R > = 463$ nm and $\phi = 8\%$ for 2 at% Ti to $< R > = 722$ nm and $\phi = 52\%$ for 8 at% Ti. Composition measurements of the γ(f.c.c.)-matrix and γ'(L1$_2$)-precipitates demonstrate that Ti substitutes for W and Al in the γ'(L1$_2$)-precipitates, increases the partitioning of W to γ'(L1$_2$), and changes the partitioning behavior of Al from a mild γ'(L1$_2$)-former to a mild γ(f.c.c.)-former. The grain boundaries in the aged alloys exhibit W-rich precipitates, most likely μ(Co$_7$W$_6$)-type, which do not destabilize the γ(f.c.c.) plus γ'(L1$_2$) microstructure within the grains. Four important benefits accrue from replacing W and Al with Ti: (i) the alloys' mass density decrease; (ii) the γ'(L1$_2$)-solvus temperature increases; (iii) the γ'(L1$_2$) volume fraction formed during aging at 1273 K (1000 °C) increases; and (iv) the 0.2% offset flow stress increases.

1. Introduction

The discovery by Sato et al. of a new class of Co-based superalloys, Co-Al-W, strengthened by a high volume fraction of γ'(L1$_2$)-precipitates formed by aging in a γ(f.c.c.)-matrix [1] has gained strong interest for potential use in high-temperature structural applications, such as discs and blades for jet-engines and land-based natural gas-fired turbines. The current material of choice for high-temperature applications is Ni-based superalloys, containing the same γ(f.c.c.) plus γ'(L1$_2$) two-phase microstructure as the newly invented Co-based alloys [2–4]. The operating temperature of jet-engine turbines has continuously increased, leading to increased power output and efficiency, largely due to improvements of Ni-based superalloys through advancements in materials processing and alloy design [2–4]. Modern Ni-based superalloys, containing between 8 and 12 alloying additions, are nearing their theoretical limit with γ'(L1$_2$)-precipitate solvus temperatures as high as ~ 1300 °C [5]. Cobalt-based superalloys containing γ'(L1$_2$)-precipitates have been shown to have solidus and liquidus temperatures 50–100 K (50–100 °C) higher than Ni-based superalloys [1,6], indicating that Co-

superalloys could, after optimal alloying and processing procedures, achieve significantly higher operating temperatures than Ni-based superalloys.

Current research on Co-superalloys has predominantly mirrored previous research on Ni-based superalloys. High-temperature creep properties for single crystals [7–14] and polycrystals [15–19] and flow-stress behavior [6,12,13,19–21] for different Co-based superalloys have been investigated, as well as dislocation behavior and stacking-fault formation of plastically deformed alloys [11,18,22–24]. Mechanical properties are largely controlled by elemental partitioning of alloying species; the effect of partitioning on the microstructure, lattice parameter mismatch, and γ(f.c.c.)-matrix plus γ'(L1$_2$)-precipitate compositions, have been measured in quaternary and some quinary alloys [25–29]. Also of particular interest is the positive lattice-parameter misfit in Co-based superalloys, which causes γ'(L1$_2$)-precipitate rafting along $< 100 >$-type directions to occur parallel to the tensile loading and perpendicular to the compressive loading directions (opposite to the behavior of Ni-based superalloys, which has a negative lattice parameter misfit), which may be beneficial to high-temperature creep

---

properties [30].

Four of the primary challenges linked with the development of Co-based superalloys are: (i) increasing the stability of the $\gamma'(L1_2)$-precipitates over a wide range of elevated temperatures; (ii) increasing the $\gamma'(L1_2)$-precipitate solvus temperatures; (iii) decreasing the mass density of the Co-superalloy; and (iv) increasing their flow stresses and creep strengths. Studies focusing on stability of the $\gamma'(L1_2)$-precipitates have suggested that this phase is metastable in the Co-Al-W ternary system [31,32]. The solvus temperature of existing Co-superalloys is often 200–300 K (200–300 °C) lower than conventional Ni-based superalloys [1,16,17,29,33,34], thereby limiting their application as high-temperature alloys for turbine blades but not discs. Additionally, Co-superalloys have mass densities greater than 9.0 g cm^{-3} [34], which is higher than the 8.4–9.1 g cm^{-3} range [35–37] typical of nickel-based superalloys.

Titanium is known to improve the high-temperature stability of the $\gamma'(L1_2)$-precipitates [19,38] and increase the creep strength of Co-based alloys [16,17]. The addition of Ni also stabilizes $\gamma'(L1_2)$-precipitates and widens the γ(f.c.c.) plus $\gamma'(L1_2)$ two-phase field [39], which is very important. The present research focuses on adding Ni and Ti to Co-Al-W alloys, focusing specifically on Co-10Ni-(9 – x)Al-(9 – x)W-2xTi at%, where x = 0, 1, 2, 3, 4 to further investigate Ti, in the presence of Ni additions, on the high-temperature stability of $\gamma'(L1_2)$-precipitates, and the $\gamma'(L1_2)$-solvus temperature and the mass density and strength of these alloys. The stability of the $\gamma'(L1_2)$-precipitates is investigated by high-temperature long-term aging experiments performed at 1273 K (1000 °C) for up to 1000 h. Phase compositions and the partitioning ratio of each alloying addition are measured by energy-dispersive X-ray spectroscopy (EDS) in samples with highly coarsened $\gamma'(L1_2)$-precipitates. Multi-temperature flow-stress tests and room-temperature Vickers microhardness measurements are utilized to determine the effects of Ti additions on the mechanical properties of the alloys. Alloy mass density is measured for each sample and compared to conventional Ni-based superalloys and low density Co-based alloys.

2. Experimental methods

Button ingots of ~ 50 g were produced with nominal compositions of Co-10Ni-(9 – x)Al-(9 – x)W-2xTi at% (x = 0, 1, 2, 3, 4) by arc-melting, under a partial Ar atmosphere, high purity Co (99.9%), Al (99.999%), Ni (99.995%), Ti (99.995%) and a Co-10Ni-9Al-9W at% master alloy. Ingots were remelted four times and flipped between each melting step to ensure a homogenous distribution of the constituent elements. Bulk compositions were measured using a Varian Vista Pro inductively coupled plasma (ICP) atomic emission spectrometer (AES) on ~ 1 g samples. Co-10Ni-(9 – x)Al-(9 – x)W-2xTi alloys with x = 0, 1, 2 were homogenized in a high-vacuum furnace at 1573 K (1300 °C) for 24 h followed by furnace cooling. Due to incipient melting at these temperatures, alloys with x = 3, 4 were homogenized at 1513 and 1493 K (1240 and 1220 °C), respectively, for 24 h followed by furnace cooling. Samples used to investigate the high-temperature stability of the $\gamma'(L1_2)$-precipitates were wrapped in Ta foil and encapsulated in quartz tubes, which were flushed with Ar and evacuated, aged at 1273 K (1000 °C) for 64, 256, or 1000 h and quenched into ice water. Samples used to measure the flow stress were wrapped in Ta foil, encapsulated in quartz tubes that were flushed with Ar and then evacuated, aged at 1173 K (900 °C) for 168 h and then air-cooled. Mass density for each alloy was measured using Archimedes' method.

Scanning electron microscopy (SEM) images and energy-dispersive X-ray spectroscopy (EDS) composition results were recorded using an Hitachi S-3400N-II SEM equipped with an Oxford INCAx-act SDD EDS detector. Samples used for SEM imaging were polished to a 1 µm finish. The average circular area-equivalent radius, < R >, and volume fraction, ϕ, for $\gamma'(L1_2)$-precipitates were measured by the line-intercept method [40] on SEM images acquired near a {100}-type plane. For an individual cuboidal γ'-precipitate, the circular area-equivalent radius is calculated from $<R> = \sqrt{\frac{A}{\pi}}$, where A is the area of the precipitate. The area equivalent number density, N_A, was measured by counting precipitates in SEM micrographs and dividing by the total area contained in the micrograph. Volumetric precipitate number density, N_v, was calculated from the area number density, N_A, from $N_v = \frac{N_A}{2 < R >}$ [40,41].

Differential thermal analysis (DTA) experiments were performed using a Netzsch STA 409C instrument to measure the $\gamma'(L1_2)$-solvus, -solidus, and -liquidus transformation temperatures. Cylindrical DTA samples ~ 4 mm long with a 5 mm diam and 0.7–0.9 g mass, were extracted from the as-cast alloys. The DTA chamber was backfilled twice with inert gas, either He or Ar, to remove oxygen before commencing to heat a sample. Single-cycle experiments at a heating rate of 10 K (10 °C) min^{-1} were used to identify the solidus and liquidus transitions. To accurately determine the $\gamma'(L12)$-solvus transition, the temperature was cycled three times through the transformation range at a heating/cooling rate of 5 K (5 °C) min^{-1}.

Vickers microhardness measurements were performed at ambient temperature utilizing a Struers Duramin-5 microhardness tester with an applied load of 1 kg and a dwell time of 5 s. Measurements were made across multiple grains, with an average grain diameter of ~ 0.5 mm, on samples that were polished to a 1 µm finish. Flow-stress measurements were performed on an MTS 810 load frame equipped with a controlled atmosphere/vacuum chamber. Cylindrical compression samples for flow stress testing, 5 mm diam × 10 mm length, were electro-discharge machined from aged buttons. The cylindrical samples were sandwiched between SiC platens lubricated by boron nitride and deformed at a constant strain rate of 10^{-4} s^{-1}. Tests were conducted in an Ar atmosphere, where the vacuum chamber was initially evacuated to 0.05 Torr and then backfilled with Ar. Multiple flow-stress measurements were performed on a single compression sample, where each compression sample was deformed to no more than 0.5% plastic strain per temperature step and the temperature was increased for each step. A thermocouple was in contact with the specimen to ensure that the sample was within ± 2 K (± 2 °C) of the desired temperature.

3. Results

3.1. Bulk alloy compositions

Aluminum and W are the primary $\gamma'(L1_2)$-formers in the Co-Al-W ternary system. Titanium is also a γ'-former [19,28,38] and the Co-Ni-(9 – x)Al-(9 – x)W-2xTi at% compositions are chosen to keep the total amount of $\gamma'(L1_2)$-forming species in the alloy constant. Herein, the alloys will be referred to by their concentration of Ti (0, 2, 4, 6 or 8 Ti at %). Bulk alloy compositions were confirmed using ICP-AES and EDS measurements and are summarized in Table 1.

3.2. Mass density

The higher mass density of current research-based Co-superalloys (> 9.0 g cm^{-3} [34]) as compared to commercial Ni-based superalloys is a key challenge for their potential use in moving parts subjected to centrifugal forces; specifically, turbine blades and discs in jet-engines. The high concentration of W in the Co-Al-W-based superalloys – typically between 7 and 10 at% W (between 20 and 27 wt%) – is the primary cause of their high mass density. Thus, reducing the amount of W necessary to form the $\gamma'(L1_2)$-precipitates without unduly decreasing their $\gamma'(L1_2)$ volume fraction, coarsening resistance, strength and solvus/solidus/liquidus temperatures is highly desirable. Recently, Makineni et al. [42,43] have introduced a new family of W-free Co-Ni-Al-Mo-Nb superalloys, with low mass densities of 8.4 g cm^{-3} and high $\gamma'(L1_2)$-precipitate fractions, where 5 Mo and 2 at% Nb replace 10 at% W. While these W-free alloys are less dense than most conventional Ni- and Co-based superalloys [35,37], the complete removal of W strongly decreases the solvus temperatures [to 1139–1263 K (866–990 °C),

Table 1

Composition of the Co-10Ni-(9 – x)Al-(9 – x)W-2xTi at% alloys as determined by inductively coupled plasma (ICP) atomic emission spectrometer (AES) and energy dispersive spectroscopy.

Alloy	Concentration (at%) ICP-AES (EDS)				
	Co	Ni	Al	W	Ti
10Ni-9Al-9W-0Ti	Bal.	10.2 (10.2 ± 0.1)	8.1 (7.9 ± 0.1)	8.9 (8.9 ± 0.1)	–
10Ni-8Al-8W-2Ti	Bal.	10.2 (9.9 ± 0.2)	7.3 (7.3 ± 0.3)	8.0 (8.7 ± 0.2)	2.2 (2.2 ± 0.1)
10Ni-7Al-7W-4Ti	Bal.	10.3 (10.1 ± 0.2)	6.3 (6.2 ± 0.4)	7.0 (7.5 ± 0.2)	4.1 (4.1 ± 0.1)
10Ni-6Al-6W-6Ti	Bal.	10.2 (10.1 ± 0.3)	5.4 (5.2 ± 0.1)	6.1 (6.7 ± 0.2)	5.9 (6.4 ± 0.1)
10Ni-5Al-5W-8Ti	Bal.	10.0 (10.4 ± 0.6)	4.5 (3.9 ± 0.1)	5.2 (4.9 ± 0.1)	7.8 (8.4 ± 0.1)

depending on the Ni content], while their coarsening resistance is largely unexplored. Likewise, partially replacing W with Ti in our Co-Ni-Al-W-Ti alloy series results in a mass density reduction; for every 1 at% W plus 1 at% Al replaced by 2 at% Ti, the alloy mass density decreases by 2%, or 0.10 g cm^{-3} (Fig. 1). Our Co-10Ni-6Al-6W-6Ti and Co-10Ni-5Al-5W-8Ti alloys have mass densities of 9.17 ± 0.03 and 8.84 ± 0.03 g cm^{-3}, respectively, which, while not as low as the W-free alloys [42,43], are well within the range of Ni-based superalloys. Additionally, the solvus temperatures in the Ti-containing alloys 1376–1403 K (1103–1130 °C) remain high compared to similar Co-based superalloys, and the peak flow-stress is also high.

3.3. Microstructural development and high-temperature stability at 1000 °C

3.3.1. γ′(L1$_2$)-precipitate microstructure

The 2, 4, 6, and 8 Ti alloys aged at 1273 K (1000 °C) for 64, 256, or 1000 h (Fig. 2) display a two-phase microstructure consisting of γ′(L1$_2$)-precipitates embedded in a γ(f.c.c.)-matrix. Neither γ′(L1$_2$)-precipitates, nor any other phases, were observed in the 0 Ti alloy indicating that the γ′(L1$_2$) solvus temperature is less than 1273 K (1000 °C). The γ′(L1$_2$)-precipitate statistics for these alloys, including the mean circular area-equivalent radius, volume fraction, and number density, are reported in Table 2. After 64 h of aging at 1273 K (1000 °C), the γ′(L1$_2$)-precipitates in each of the alloys exhibit a primarily cuboidal morphology. The γ′(L1$_2$)-precipitates in the 4, 6, and 8 Ti alloys are aligned along < 100 > -type directions, whereas the γ′(L1$_2$)-precipitates in the 2 Ti alloy are more randomly distributed. After 256 h of aging, the γ′(L1$_2$)-precipitates in the 2, 4, 6, and 8 Ti alloys are all aligned strongly along < 100 > -type directions. The γ′(L1$_2$)-precipitates in the 2 and 4 Ti alloys maintain their cuboidal morphology. In contrast, the precipitates in the 6 and 8 Ti alloys coalesce and become highly interconnected after 256 h of aging, while maintaining their preferred < 100 > crystallographic direction. In this case, the γ′(L1$_2$)-precipitates
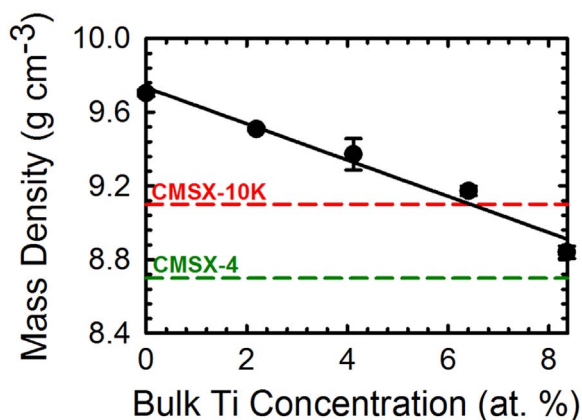

Fig. 1. Mass density, measured by Archimedes' method, of the Co-10Ni-(9 – x)Al-(9 – x)W-2xTi at% alloys (black). Values for commercial Ni-base superalloys CMSX-4 and CMSX-10K are from Ref. [37].

have a high aspect ratio (typically greater than 2:1) irregularly-shaped cross-sections, while maintaining some cuboidal faceting characteristic of the earlier aging times. The precipitate morphology after 1000 h of aging is similar to the microstructure in the alloys aged for 256 h, but the precipitates are 10–50% larger due to their continuous coarsening. The γ′(L1$_2$)-precipitates in the 2 and 4 Ti alloys are distinguishable from one another by narrow γ(f.c.c.)-matrix channels that are visible between γ′(L1$_2$)-precipitates, but are more spherical at 1000 h than at shorter aging times. The γ′(L1$_2$)-precipitates in the 6 and 8 Ti alloys continue to coalesce, with two or more smaller γ′(L1$_2$)-precipitates joining to form larger γ′(L1$_2$)-precipitates similar to what has been found in Ni-based superalloys [44].

The calculated γ′(L1$_2$)-precipitate characteristics are presented in Fig. 3. The coarsening rate constant, K, and temporal exponent, p, were calculated from the coarsening-rate equation first described by Lifshitz and Slyozov [45] and Wagner [46] (LSW):

$$\langle R(t) \rangle^p - \langle R(t_0) \rangle^p = K(t - t_0) \qquad (1)$$

utilizing two methods (Table 3): (i) linear regression where p was set equal to 3 [45] and (ii) a nonlinear multi-variate regression analysis calculated in *SigmaPlot* [47]. t_0 is the time at the onset of quasi-stationary coarsening, t is the aging time, and $\langle R(t) \rangle$ is the mean γ′(L1$_2$)-precipitate radius at time t. Using the linear regression method, the rate constant, K, increases with the concentration of Ti, where K for the 2, 4, 6, 8 Ti alloys is equal to 3.6, 2.9, 9.1, and 16.6 × 10^{-26} m^3 s^{-1}, respectively, thereby showing that reducing the concentrations of W and Al and increasing the concentration of Ti increases the coarsening kinetics in Co-base superalloys. Using the multi-variate regression method, the inverse of the temporal exponent, (1/p in Eq. (1)) for the 2, 4, 6, and 8 Ti alloys were calculated to be 0.22 ± 0.05, 0.24 ± 0.03, 0.27 ± 0.10 and 0.29 ± 0.12, respectively, with corresponding coarsening rate constants calculated as 94.8 m$^{\frac{1}{0.22}}$ s^{-1}, 89.0 m$^{\frac{1}{0.24}}$ s^{-1}, 98.2 m$^{\frac{1}{0.27}}$ s^{-1}, and 104.2 m$^{\frac{1}{0.29}}$ s^{-1}. These values are difficult to interpret since the variation in temporal exponent lead to inconsistent units for the coarsening rate constants. The γ′(L1$_2$) volume fraction, $\phi(t)$, increases with increasing Ti concentration (Fig. 3b), ranging from 8 ± 3% in the 2 Ti alloy to 50 ± 3% in the 8 Ti alloy, due to continuously increasing solvus temperatures resulting from the Ti additions. The $\phi(t)$ values remain stable with aging time through 1000 h, where the average standard deviation for all alloys is 2.8%. Additionally, the number density, N$_v$(t), (Fig. 2c) decreases continuously with increasing aging time for the 2 and 4 Ti alloys as the γ′(L1$_2$) precipitates coarsen; after an initial decrease from 64 to 256 h, N$_v$(t) is constant from 256 to 1000 h in the 6 and 8 Ti alloys.

3.3.2. Phase concentrations

γ(f.c.c.)- and γ′(L1$_2$)-phase compositions were measured using EDS in samples aged at 1273 K (1000 °C) for 1000 h (Fig. 4). EDS measurements were recorded for the wide γ(f.c.c.)-channels and highly coarsened γ′(L1$_2$)-precipitates to minimize the electron-beam overlapping both phases. The bulk alloy Ti concentration has a significant effect on the composition of the γ(f.c.c.)-matrix (Fig. 4a). The Co-rich
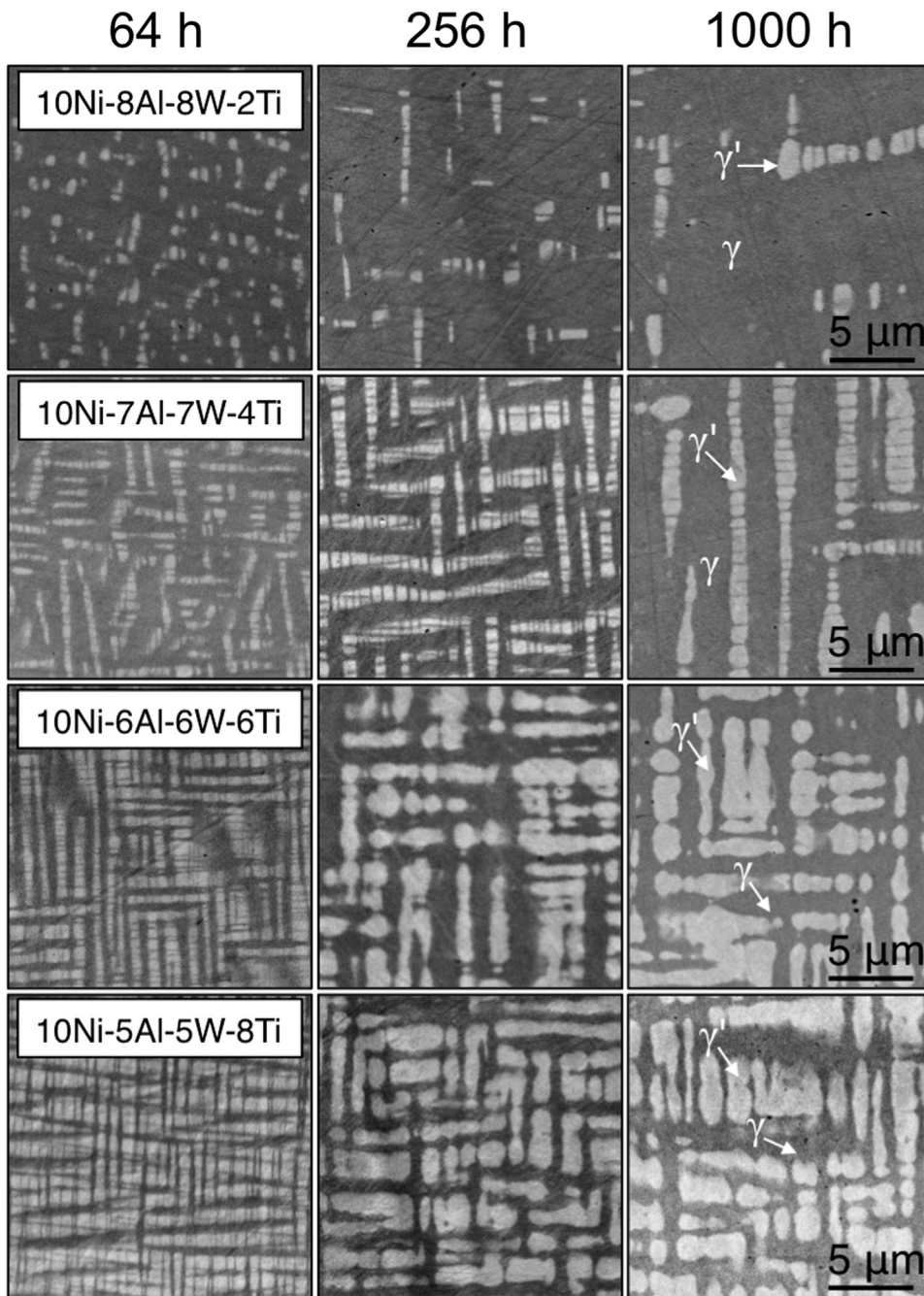
Fig. 2. Backscattered scanning electron microscope micrographs of the γ(f.c.c.) plus γ′(L1$_2$) microstructure in the Co-10Ni-(9 − x)Al-(9 − x)W-2xTi at% alloys aged at 1273 K (1000 °C) for 64, 256, and 1000 h.

matrix becomes slightly more enriched, increasing by 2.5 at% Co from 73.0 ± 0.2 (0 Ti) to 75.5 ± 1.0 (8 Ti) at% Co. The Ni concentration displays a relative decrease of 10% (1.1 at% from 10.6 ± 0.2–9.5 ± 0.2 at% Ni), while the W and Al concentrations are the most strongly affected, decreasing by about a factor 2 (52% and 49% reductions, respectively). Finally, the Ti concentration in the γ(f.c.c.)-matrix increases from 0 to 6.7 at%, at a slightly lower rate than the overall bulk Ti-concentration, that is, increasing by 0.8 at% per 1 at % Ti added to the bulk alloy. With the exception of Co, the change in the γ(f.c.c.)-matrix composition is linear with the change in bulk Ti concentration.

In the γ′(L1$_2$)-precipitates (Fig. 4b), the concentration of Co and Ni remains stable for all alloys at 67.3 ± 0.4 and 10.8 ± 0.2, respectively; however, the concentrations of W, Al, and Ti change significantly. In the Co-10Ni-(9 − x)Al-(9 − x)W-2xTi at% alloys the concentrations of W and Al in the γ′(L1$_2$)-precipitates both decrease by 0.7 at% per 1 at% Ti

addition to the bulk alloy composition. Conversely, the concentration of Ti in the γ′(L1$_2$)-precipitates increases by 1.3 at% per 1 at% Ti addition, effectively compensating for the decrease of both W and Al in the γ′(L1$_2$)-precipitates, which totals 1.4 at% per 1 at% Ti. Thus, confirming that Ti is substituting for both W and Al in the γ′(L1$_2$)-precipitates.

The partitioning ratio $K_i^{\gamma'/\gamma}$, was calculated as the ratio of the atomic concentrations of element i in the γ′(L1$_2$)-precipitates to its atomic concentration in the γ(f.c.c.)-matrix ($\frac{C_i^{\gamma'}}{C_i^{\gamma}}$) (Fig. 5), for each atomic species for all samples aged for 1000 h. A value of $K_i^{\gamma'/\gamma}$ greater than unity indicates that species i is a γ′(L1$_2$)-former, a value less than unity indicates that it is a γ(f.c.c.)-matrix former, and a value of unity indicates that species i partitions equally to the γ′(L1$_2$)- and γ(f.c.c.)-phases. The partitioning ratio of Ti remains constant for all alloys at 1.71 ± 0.03. The partitioning ratio of W increases substantially from 2 Ti (1.23 ± 0.02) to 8 Ti (1.50 ± 0.03), even though the 8 Ti alloy

Table 2

Area equivalent mean radius, $< R(t) >$, volume fraction, $\phi(t)$, and number density, $N_v(t)$, of the $\gamma'(L1_2)$-precipitates, and bulk Vickers microhardness and mass density of the Co-10Ni-(9 – x)Al-(9 – x)W-2xTi at% alloys after aging at 1273 K (1000 °C) for 64, 256, and 1000 h.

Alloy	Aging time at 1000 °C (h)	$< R >$ (nm)	ϕ (%)	N_v (10^{17} # m^{-3})	Vickers hardness (GPa)	Density (g cm^{-3})
10Ni-9Al-9W-0Ti	64 h	–	–	–	2.26 ± 0.13	9.70 ± 0.02
	256 h	–	–	–	2.34 ± 0.08	
	1000 h	–	–	–	2.49 ± 0.08	
10Ni-8Al-8W-2Ti	64 h	250 ± 63	11 ± 2	12.6 ± 3.3	2.93 ± 0.05	9.51 ± 0.01
	256 h	302 ± 69	6 ± 2	3.7 ± 0.9	2.97 ± 0.11	
	1000 h	463 ± 160	8 ± 1	1.1 ± 0.4	2.92 ± 0.06	
10Ni-7Al-7W-4Ti	64 h	244 ± 57	19 ± 3	26.8 ± 6.2	3.00 ± 0.06	9.37 ± 0.09
	256 h	319 ± 98	26 ± 4	16.8 ± 5.1	3.01 ± 0.07	
	1000 h	471 ± 139	24 ± 3	3.0 ± 0.9	3.00 ± 0.07	
10Ni-6Al-6W-6Ti	64 h	283 ± 69	39 ± 5	41.7 ± 10.1	2.96 ± 0.08	9.17 ± 0.03
	256 h	539 ± 322	37 ± 2	2.1 ± 1.3	2.86 ± 0.05	
	1000 h	595 ± 349	41 ± 3	2.2 ± 1.3	2.84 ± 0.06	
10Ni-5Al-5W-8Ti	64 h	324 ± 72	51 ± 3	36.6 ± 8.4	3.07 ± 0.04	8.84 ± 0.03
	256 h	673 ± 306	47 ± 3	1.9 ± 0.9	3.11 ± 0.06	
	1000 h	722 ± 336	52 ± 4	1.8 ± 0.8	2.90 ± 0.06	
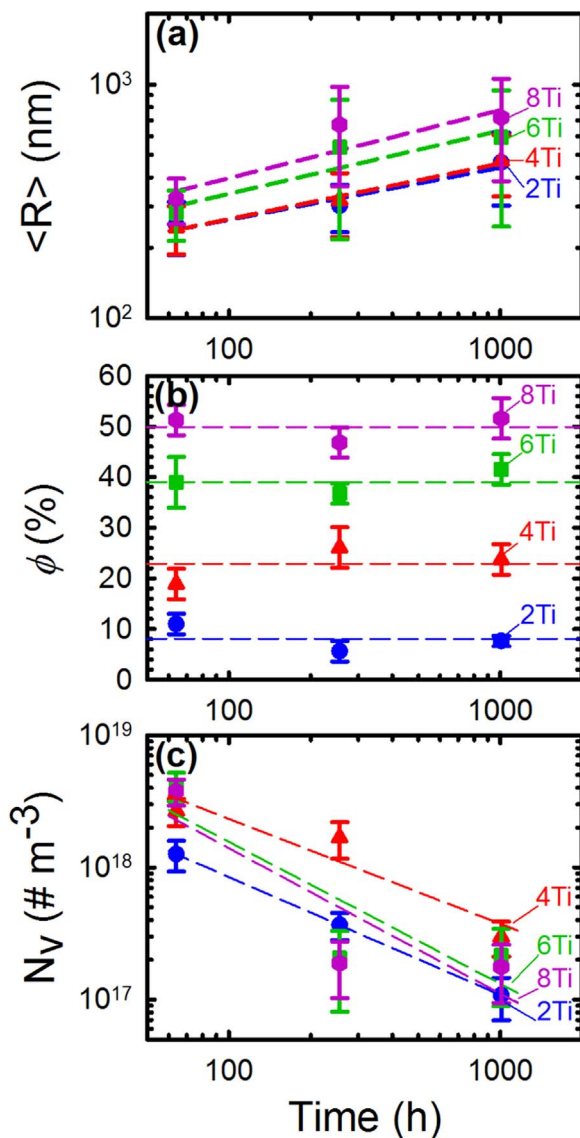
Fig. 3. $\gamma'(L1_2)$-precipitate: (a) area equivalent mean radius (nm); (b) volume fraction (%); and (c) number density (# m^{-3}) in the Co-10Ni-(9 – x)Al-(9 – x)W-2xTi at% alloys aged at 1273 K (1000 °C) for 64, 256, or 1000 h.

Table 3

Calculated temporal exponent, p, and coarsening rate constant, K, using linear regression and nonlinear multi-variate regression methods.

Alloy	Linear regression $\frac{1}{p} = \frac{1}{3}$	Multi-variate regression analysis	
	$K \times 10^{-26}$ m^3 s^{-1}	$\frac{1}{p}$	$K \times 10^{-26}$
10Ni-9Al-9W-0Ti	–	–	–
10Ni-8Al-8W-2Ti	3.6	0.22	94.8 m$^{\frac{1}{0.22}}$ s^{-1}
10Ni-7Al-7W-4Ti	2.9	0.24	89.0 m$^{\frac{1}{0.24}}$ s^{-1}
10Ni-6Al-6W-6Ti	9.1	0.27	98.2 m$^{\frac{1}{0.27}}$ s^{-1}
10Ni-5Al-5W-8Ti	16.6	0.29	104.2 m$^{\frac{1}{0.29}}$ s^{-1}

contains only 5 at% W (the smallest of all the alloys). The partitioning ratio of Al decreases with increasing Ti content, with Al preferring the $\gamma'(L1_2)$-phase for the 2 Ti, 4 Ti and 6 Ti alloys, and partitioning weakly to the γ(f.c.c.)-matrix in the 8 Ti alloy. The partitioning ratio of Ni increases slightly with increasing Ti concentration, from 1.03 ± 0.03–1.14 ± 0.03, and the partitioning ratio of Co decreases slightly, from 0.93 ± 0.01–0.89 ± 0.01.

3.3.3. Heterogeneous precipitation at grain boundaries

Micron-sized (1–3 μm) semi-continuous grain boundary (GB) precipitates are observed in all alloys on nearly all of the GBs after 256 h of aging at 1273 K (1000 °C), Fig. 6. After 1000 h of aging, the GB precipitates are still present at the GBs of the 0 and 2 Ti alloys, but less so for the 4, 6, and 8 Ti alloys, implying that the GB precipitates may be metastable. On either side of the GB there is a precipitate-denuded zone (PDZ), 2–20 μm wide, that contains no precipitates (observed using SEM), $\gamma'(L1_2)$ or otherwise. The GB precipitates do not appear to affect the two-phase (f.c.c.) plus $\gamma'(L1_2)$ microstructure in the grain interior beyond the PDZ. There is a small fraction (about 1–2%) of needle-shaped precipitates in the 6 Ti alloy aged at 1273 K (1000 °C) for 256 h, typically in regions near the GB; their composition is Co-26W-11Ti-5Ni-1Al at% and they are identified to be $Co_3W(D0_{19})$, with Ti, Ni and Al substituting for Co. Fig. 7a displays a concentration profile across the width of a GB precipitate in the 8 Ti alloy. The GB precipitates are enriched in W causing the surrounding PDZ to be W-deficient. Nickel and Al partition strongly away from the GB-precipitate with only a small concentration of either element remaining in the precipitate. The composition of the GB precipitate in the base Co-10Ni-9Al-9W alloy is 52 at% Co and 45 at% W and it contains small concentrations of Ni and
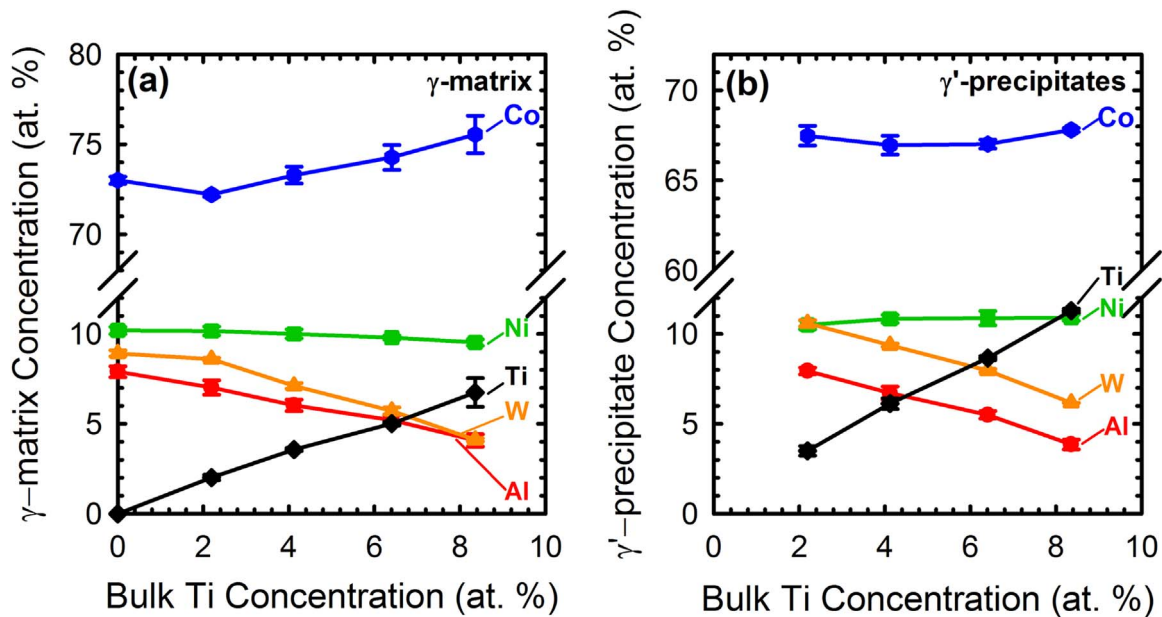
Fig. 4. Energy dispersive spectroscopy measurements of the composition of the: (a) γ(f.c.c.)-matrix; and (b) γ′(L1$_2$)-precipitates in Co-10Ni-(9 – x)Al-(9 – x)W-2xTi at% alloys aged at 1273 K (1000 °C) for 1000 h as a function of the bulk Ti concentration.
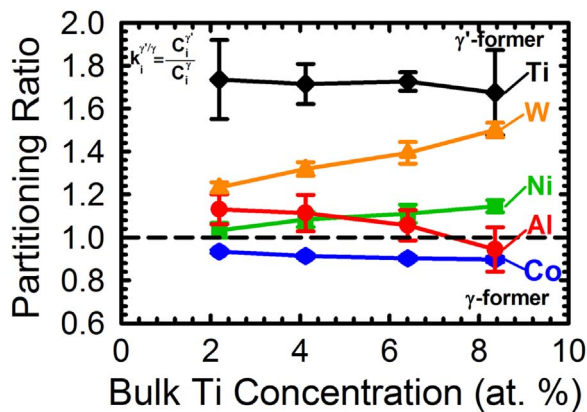

Fig. 5. Partitioning ratio of, $K_i^{\gamma'/\gamma} = \frac{c_i^{\gamma'}}{c_i^{\gamma}}$, of Co-10Ni-(9 – x)Al-(9 – x)W-2xTi at% alloys aged at 1273 K (1000 °C) for 1000 h.

Al (2.4 and 0.6 at%). This composition is very close to the stoichiometry of the μ(Co$_7$W$_6$)-phase, which is known to form in Co-superalloys [32]. The concentrations of Co, Ni, and Al (Fig. 7b) in the precipitates remain constant for all alloys at 51.8 ± 1.0 Co, 3.0 ± 0.5 Ni, and 0.7 ± 0.5 Al at%, respectively. When the Ti concentration is increased and the W and Al concentrations are decreased in the bulk alloy, Ti substitutes for W, with the W plus Ti sum remaining constant at 44.5 ± 1.7 at% and the composition of the μ-phase changing to Co$_7$(W$_{1-0.09x}$Ti$_{0.09x}$)$_6$ for x equals 0–4, when ignoring the small concentrations of Ni and Al.

3.4. Microstructural development of alloy aged at 900 °C

Samples used for high-temperature flow-stress tests were aged at 1173 K (900 °C) for 168 h and then air-cooled. The microstructure in all of the alloys contained a high volume fraction of the cuboidal γ′(L1$_2$)-precipitate phase embedded in a γ(f.c.c.)-matrix (Fig. 8). The volume fraction of γ′(L1$_2$)-precipitates in the alloys aged at 1173 K (900 °C) (Fig. 9) is greater than in the alloys aged at 1273 K (1000 °C) (Fig. 9) ranging from 56% in the 0 Ti alloy to 68% in the 8 Ti alloy. The mean precipitate radius (Fig. 9) increases with increasing Ti concentration, from 84 ± 12 nm in the 0 Ti alloy to twice this value (162 ± 32 nm) in

the 8 Ti alloy, but < R(t) > is ~ 5 times smaller than in the same alloys aged at 1273 K (1000 °C). The GBs do not contain the W-rich precipitates observed at 1273 K (1000 °C) (Fig. 2), but rather consist primarily of coarsened γ′(L1$_2$)-precipitates (Fig. 8). There are occasional examples of Ti-rich Co-28Ti-10W-3Ni-2Al precipitates at the GBs in the 6 Ti alloy, possibly Co$_2$Ti-type [48].

3.5. Solvus, solidus and liquidus temperatures

The γ′(L1$_2$)-precipitate solvus temperature and the solidus and liquidus temperatures were measured by differential thermal analysis (DTA) (Fig. 10a). The γ′(L1$_2$) solvus temperature increases near linearly with bulk Ti concentration from 1255 K (982 °C) in the 0 Ti alloy to 1410 K (1137 °C) in the 8 Ti alloy (Fig. 11). The solidus and liquidus temperatures both decrease near linearly with increasing Ti concentration, from 1732 K (1459 °C) and 1762 K (1489 °C) in the 0 Ti alloy to 1550 K (1277 °C) and 1656 K (1383 °C) in the 8 Ti alloy. These decreasing temperatures with increasing Ti concentration are probably due to the reduction in the high-melting-point W concentration as the Ti additions increase. The width of the solid-liquid temperature interval increases from 30 K (30 °C) in the 0 Ti alloy to 106 K (106 °C) in the 8 Ti alloy.

For all alloys, peaks present below the γ′(L1$_2$) solvus peak, denoted in this work as low-temperature peaks, are observed between 923 K (650 °C) and 1073 K (800 °C) (Fig. 10b). Similar low-temperature peaks were observed by Zenk et al. in Co-Al-W-Ti alloys, ranging from Co-9Al-8W-0Ti to Co-0Al-0W-12Ti, and were attributed to the dissolution of secondary γ′(L1$_2$)-precipitates [19]. Multi-temperature aging studies performed by Kobayashi et al. on Co-Al-W-Ti alloys, ranging from Co-9.4Al-9.6W-0Ti to Co-0Al-0W-16.5Ti, found that CoAl(B2) and Co$_2$(Al,Ti) β-precipitates form in equilibrium with the γ(f.c.c.) and γ′(L1$_2$) phases below 1173 K (900 °C) [38]. In the present study, CoAl (B2) precipitates are not observed in any of the alloys, and thus the lower-temperature peaks are most likely due to the dissolution of small secondary γ′(L1$_2$)-precipitates, similar to results found in Ni-based alloys [49].

Linear extrapolation of the solvus and solidus curves indicate that Co-10Ni-3.5Al-3.5W-11Ti is the highest Ti concentration for this alloy series for which γ(f.c.c.) forms a single-phase, which is useful for homogenization and solutionizing before aging. The extrapolated
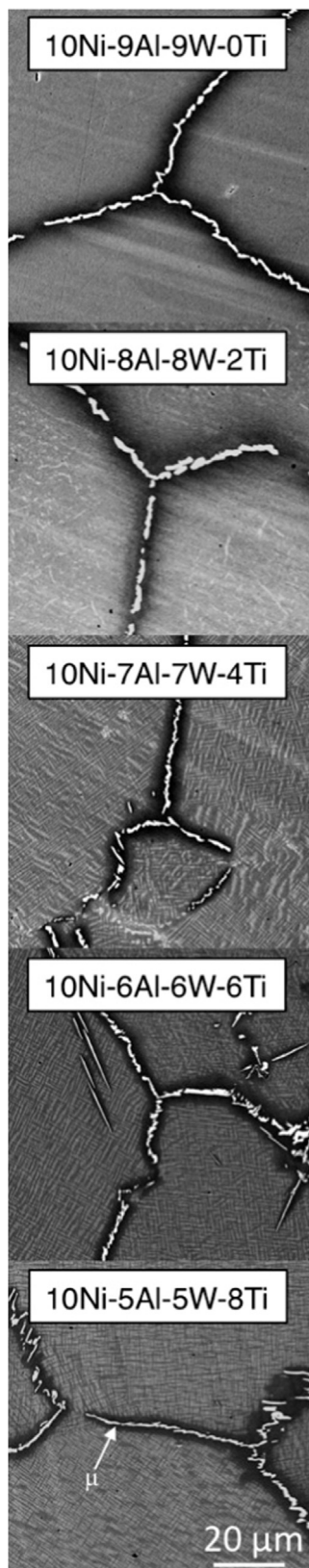
Fig. 6. Backscattered scanning electron microscope micrographs displaying the presence of W-rich grain boundary precipitates (white contrast) in Co-10Ni-(9 − x)Al-(9 − x)W-2xTi at% alloys aged at 1273 K (1000 °C) for 256 h.

liquidus temperature is, however, quite low, 1613 K (1340 °C). Additionally, further experiments are needed to confirm that no other phases exist in this low W concentration alloy.
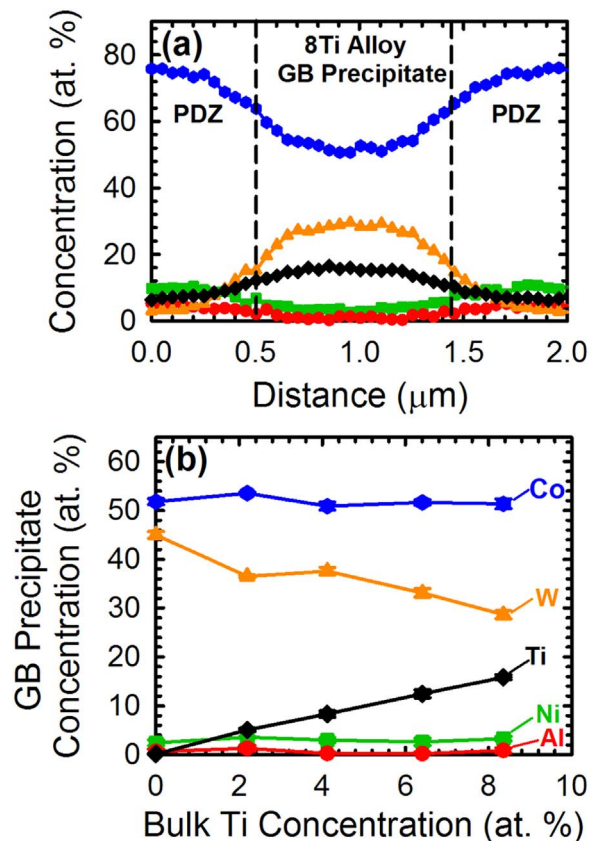

Fig. 7. Electron energy dispersive measurements of the composition of the grain boundary precipitates in Co-10Ni-(9 − x)Al-(9 − x)W-2xTi at% alloys aged at 1273 K (1000 °C) as: (a) a function of bulk Ti concentration; and (b) example of a concentration profile taken across the width of a grain boundary precipitate in the Co-10Ni-5Al-5W-8Ti at% alloy.

3.6. Mechanical properties

3.6.1. Microhardness measurements

After aging at 1273 K (1000 °C) at 64 h, the 2, 4, 6, and 8 Ti at% alloys have similar Vickers microhardness values, ranging from 2.93 ± 0.05 GPa for the 2 Ti alloy to 3.07 ± 0.04 GPa for the 8 Ti alloy (Fig. 12). For all aging times at 1273 K (1000 °C), the microhardness values of the 2 Ti (2.94 ± 0.03 GPa) and 4 Ti (3.00 ± 0.01 GPa) alloys remain constant within two standard deviations. The microhardness of the 6 Ti alloy decreases slightly from 2.95 ± 0.07–2.84 ± 0.06 GPa after 64 and 1000 h of aging, respectively. A similar small decrease is present in the 8 Ti alloy, where the microhardness value decreases from 3.07 ± 0.04–2.90 ± 0.06 GPa. These small decreases in microhardness are most likely due to an increase in the γ(f.c.c.)-matrix channel width resulting from the highly coagulated γ'(L1$_2$)-precipitate morphology observed after 256 h of aging. The microhardness of the 0 Ti alloy (2.26 ± 0.13 GPa) after 64 h is much smaller than for the other alloys due to a lack of γ'(L1$_2$)-precipitation; the microhardness increases, however, steadily with aging time, reaching 2.49 ± 0.08 GPa after 1000 h, which may indicate clustering or the presence of nanoscale γ'(L1$_2$)-precipitates that are too small to be observed via SEM.

Vickers microhardness values, measured at ambient temperature, for the alloys aged at 1173 K (900 °C) (Fig. 12) are ~ 20% higher than for the alloys aged at 1273 K (1000 °C), due to the higher volume fractions (56–68%) of γ'(L1$_2$)-precipitates present in the former alloys aged at lower temperatures. The microhardness of the 0 Ti alloy (3.04 ± 0.06 GPa) is significantly smaller than the other alloys due to its smaller volume fraction of γ'(L1$_2$)-precipitates and the absence of Ti as a solid-solution strengthening element in both the γ(f.c.c.) and
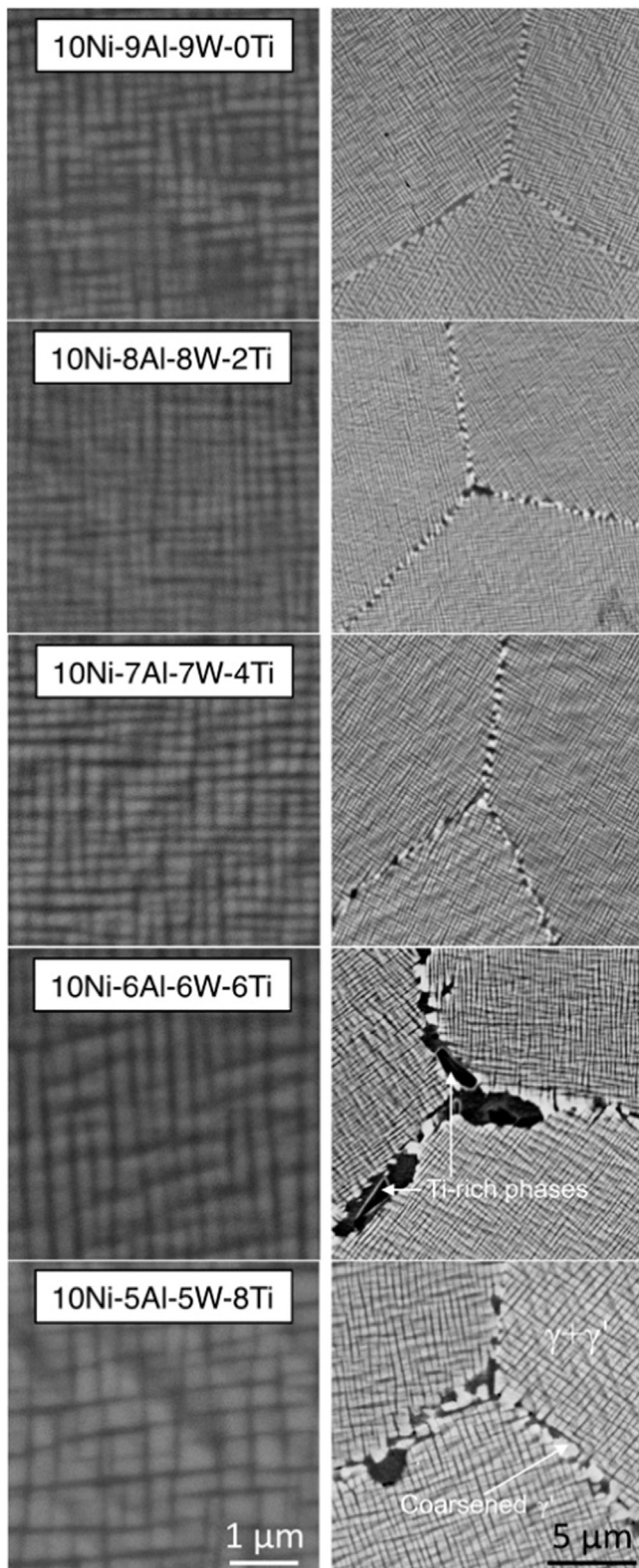
Fig. 8. Backscattered scanning electron microscope micrographs of the γ(f.c.c.) plus γ′(L1$_2$) microstructure in Co-10Ni-(9 – x)Al-(9 – x)W-2xTi at% alloys aged at 1173 K (900 °C) for 168 h (left-hand side) and representative grain boundaries from each sample (right-hand side), corresponding to the samples used for the flow-stress measurements.

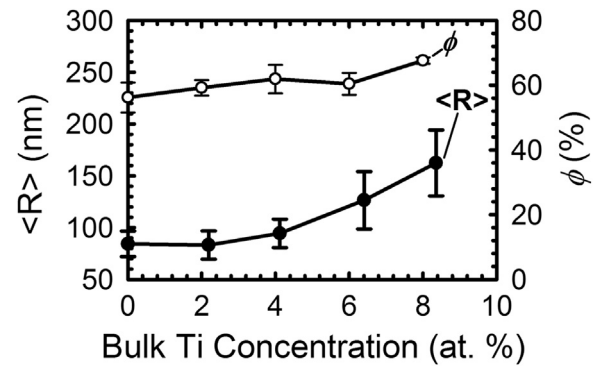Fig. 9. Area equivalent mean radius and volume fraction of γ′(L1$_2$)-precipitates in the Co-10Ni-(9 – x)Al-(9 – x)W-2xTi at% alloys aged at 1173 K (900 °C) for 168 h corresponding to the samples used for flow-stress measurements.
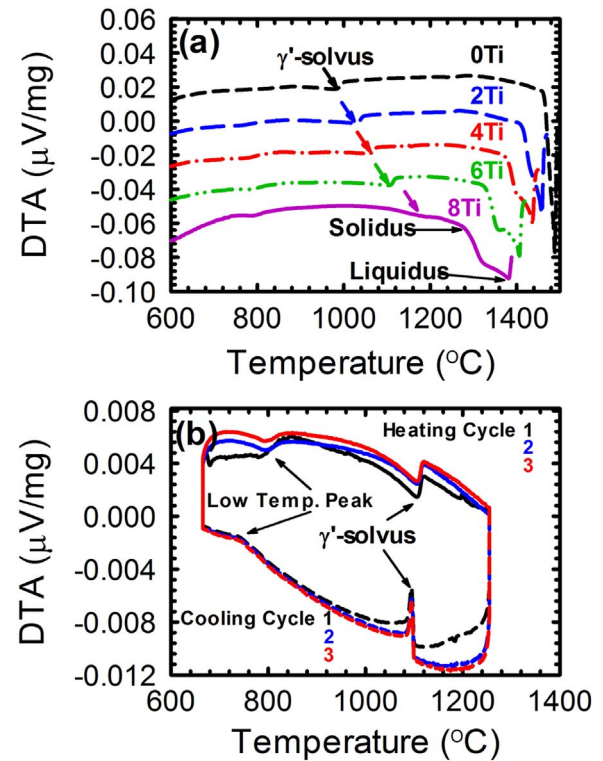

Fig. 10. Differential thermal analysis heating curves displaying: (a) solvus, solidus, and liquidus transitions in Co-10Ni-(9 – x)Al-(9 – x)W-2xTi alloys for a heating rate of 10 °C min^{-1}; and (b) a triple cycled heating experiment displaying a low-temperature peak and γ′(L1$_2$)-solvus temperature during heating (solid-line) and cooling (dashed-line) at a heating/cooling rate of 5 °C min^{-1} in a Co-10Ni-6Al-6W-8Ti at% alloy.

γ′(L1$_2$) phases. The microhardness values gradually increase from 3.59 ± 0.08 GPa in the 2 Ti alloy to 3.72 ± 0.11 GPa in the 6 Ti alloy before decreasing slightly to 3.54 ± 0.10 GPa in the 8 Ti alloy. The microhardness value is independent of aging time and < R(t) > for

aging times from 64 to 1000 h. Given the correlation between microhardness, yield stress, and ultimate tensile strength (UTS) [50,51], this indicates that the alloys have been aged to peak strength, which is given by $\sim \frac{\gamma_{APB}\phi^{\frac{1}{2}}}{2b}$ [2], where γ_{APB} is the antiphase boundary energy (APB), and b is the magnitude of the Burgers vector.

3.6.2. Flow stress

Multi-temperature flow-stress tests were performed at temperatures ranging from room temperature to 1173 K (900 °C) on the alloys aged at 1173 K (900 °C) for 168 h (Fig. 13). Two samples were tested for each alloy, except for the 6 Ti alloy. The first sample was tested at temperatures from room temperature to 1023 K (750 °C) and the second sample was tested at temperatures from 1023 K (750 °C) to 1173 K (900 °C), so that flow stress was measured twice at 1023 K (900 °C)
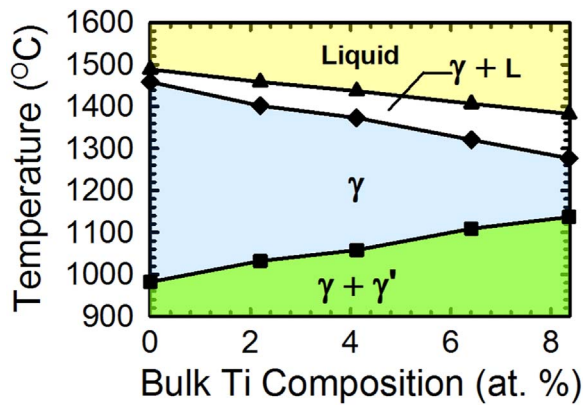
Fig. 11. Solvus, solidus, and liquidus temperatures determined from the differential thermal analysis heating curves recorded using a heating rate of 5 °C min⁻¹ for Co-10Ni-(9 – x)Al-(9 – x)W-2xTi at% alloys.
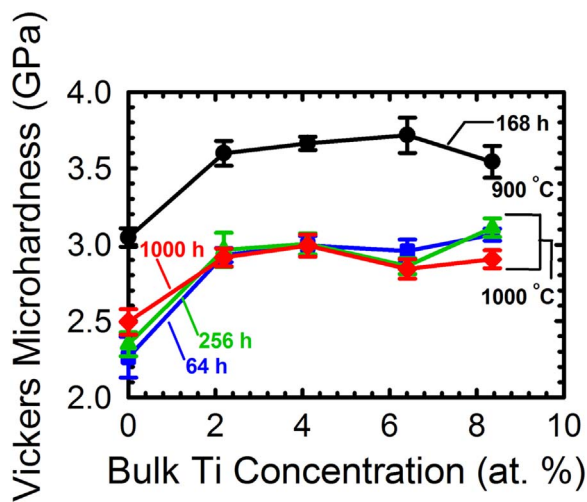

Fig. 12. Room-temperature Vickers microhardness measurements of Co-10Ni-(9 – x)Al-(9 – x)W-2xTi at% alloys aged at 1273 K (1000 °C) for 64, 256, and 1000 h and at 1173 K (900 °C) for 168 h.
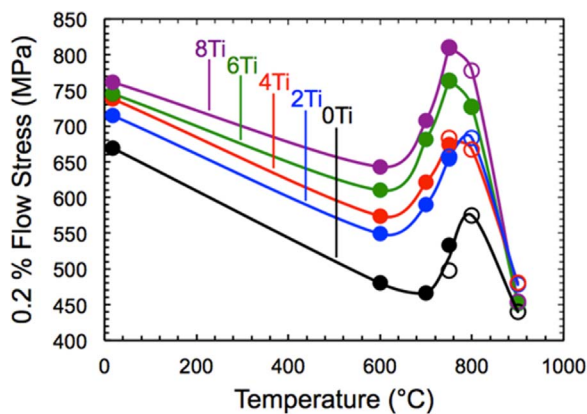

Fig. 13. Flow-stress measurements performed on Co-10Ni-(9 – x)Al-(9 – x)W-2xTi at% alloys aged at 1173 K (900 °C) for 168 h at temperatures between room temperature and 1173 K (900 °C) at a strain rate of 10⁻⁴ s⁻¹. Different samples of the same alloy are delineated with open and closed symbols of the same color. (For interpretation of the references to color in this figure legend, the reader is referred to the web version of this article.)

(750 °C). The difference in the flow stress measured at 1023 K (750 °C) for the two samples is 6.9% for the 0 Ti alloy and 0.1–0.5% for the 2,4, and 8 Ti alloys, demonstrating that strain hardening does not affect the

results. A flow stress anomaly is present in all alloys typically starting at ~ 873 K (~ 600 °C) and ending at ~ 1173 K (~ 900 °C). The replacement of Al and W by Ti significantly increases the strength of these Co-superalloys at all temperatures, through 1173 K (900 °C). The flow stress at room temperature increases by 14% from 669 MPa in the 0 Ti alloy to 762 MPa in the 8 Ti alloy. The strengthening increment induced by Ti becomes more pronounced at elevated temperatures. The peak stress of the 8 Ti alloy (810 MPa) is 30% higher than the peak stress of the 0 Ti alloy (575 MPa). Titanium also shifts the peak temperature to lower values; alloys with smaller Ti concentrations (0–2 Ti) have peaks at ~ 1073 K (~ 800 °C) in contrast to the alloys with higher Ti concentrations (4 Ti, 6 Ti, and 8 Ti), which exhibit peaks at ~ 1023 K (~ 750 °C).

4. Discussion

4.1. Stability of the $\gamma'(L1_2)$-precipitate phase

The stability of the $\gamma'(L1_2)$-precipitate phase in Co-based superalloys is critical for their applicability as high-temperature structural materials. Originally, the $\gamma'(L1_2)$-phase in ternary Co-Al-W alloys was thought to be stable, but later work demonstrates it is most likely metastable [31,32]. The addition of Ni has been shown to widen the γ(f.c.c.) plus $\gamma'(L1_2)$ phase-field and stabilize the $\gamma'(L1_2)$-phase [39]. The present work adds to the database for long-term stability and demonstrates that the addition of Ni and Ti (when decreasing W and Al) to a base Co-Al-W alloy results in $\gamma'(L1_2)$-precipitates that are stable after 1000 h of aging at 1273 K (1000 °C). The addition of Ti plays a crucial role in Co-based superalloys, permitting a reduction of W (thus reducing mass density, Fig. 1), while simultaneously increasing the $\gamma'(L1_2)$ volume fraction and increasing strength (Figs. 3 and 13). The addition of Ti increases the coarsening rate constants of $\gamma'(L1_2)$ precipitates (Fig. 3), which is undesirable for strength at ambient and elevated temperatures; significant gains in the high-temperature yield strength are, however, realized through Ti additions, outweighing the possible negative effects of coarsening. Also, the lack of changes in microhardness when aging at 1273 K (1000 °C) from 64 to 1000 h (Fig. 12), despite the concomitant increase in the mean radii, $< R >$, of the $\gamma'(L1_2)$-precipitates, indicates that the effect of Ti on coarsening rate does not result in a lower strength. After 1000 h at 1273 K (1000 °C) the $\gamma'(L1_2)$-precipitates become rounded and lose their cuboidal morphology but retain their rafted geometry, which may have negative implications on the mechanical properties at elevated temperature. Co-based superalloys have a positive lattice parameter misfit at ambient temperature, which becomes smaller with increasing temperature and may approach zero [30]. This decrease in lattice strain energy explains the transition from cuboids-to-rounded precipitate morphology as the precipitates coarsen.

The GBs in each of the Co-Ni-Al-W-Ti alloys aged at 1273 K (1000 °C) contain W-rich $\mu(Co_7W_6)$-precipitates. While the $\mu(Co_7W_6)$-precipitates do not appear to affect the γ(f.c.c.) plus $\gamma'(L1_2)$ phases in the grain interiors, beyond creating PDZs, their presence is of concern for long-term stability, GB strength and toughness, and environmental resistance. GBs are brittle in Co-superalloys [15,17,21,52] and the presence of $\mu(Co_7W_6)$-type GB precipitates could increase the tendency for brittle fracture or serve as nucleation sites for undesirable precipitates [16,53,54]. Thus, further studies of GB segregation and precipitation behavior with and without GB-segregating elements, such as B, C, and Zr [16,17,52,55] is needed for the practical development of polycrystalline Co-superalloys.

4.2. Solvus temperatures

The solvus temperatures of the Co-Ni-Al-W-Ti alloys range from 1258 K (985 °C) in the 0 Ti alloy (highest in W content) to 1403 K (1130 °C) in the 8 Ti alloy. To date, the highest $\gamma'(L1_2)$-precipitate

solvus values in Co-superalloys were measured in alloys containing both Ti and Ta: Co-9Al-8W-2Ta-2Ti (1426 K or 1153 °C) [17], Co-7Al-8W-4Ti-1Ta (1404 K or 1131 °C) [56], and Co-7Al-7W-4Ti-2Ta (1430 K or 1157 °C) [56]. The Co-10Ni-5Al-5W-8Ti alloy with the highest Ti and lowest W concentrations in this study, has a solvus temperature of 1403 K (1130 °C), equal to the above Co-7Al-8W-4Ti-1Ta alloy and only ~ 30 °C lower than the Co-9Al-8W-2Ta-2Ti and Co-7Al-7W-4Ti-2Ta alloys; our 8 Ti alloy contains 2–3 at% less W and is estimated to be 8% less dense. Further partial replacement of W with the potent solvus temperature-raisers, Ta and/or Nb, in these alloys may further improve their solvus temperatures [29].

4.3. Mechanical properties

The replacement of W and Al with Ti resulted in higher flow stresses for our alloys at both ambient and elevated temperatures, but has little impact on microhardness. The ambient-temperature yield strength improves by 7% from the 0 Ti to 2 Ti alloy, and then by 6% from 2 Ti to 8 Ti. The flow stress at elevated temperatures increases by 20% from 0 Ti to 2 Ti, and then by 12% from 2 Ti to 8 Ti. Titanium strengthens the alloys primarily by increasing the γ'(L1$_2$)-precipitate volume fraction from 56% (for 0 Ti) to 68% (for 8 Ti). Additionally, Ti provides solid-solution strengthening in the γ(f.c.c.)-matrix, and is in particular likely to alter the antiphase boundary (APB) and stacking fault energies of the γ'(L1$_2$)-precipitates, as is the case for the Ni-based alloys [57,58]; thereby further inhibiting dislocations from shearing the precipitates. Zenk et al. measured flow stresses of Co-Al-W-Ti alloys, ranging from Co-9Al-8W-0Ti to Co-0Al-0W-12Ti, where the anomalous peak stress occurs at 1023 K (750 °C), ranging from 350 to 600 MPa [19]. In our Co-Ni-Al-W-Ti alloys, the anomalous peak flow stresses occur at 1023–1073 K (750 or 800 °C), similar to Zenk et al., but our flow stress values are much higher, ranging from 575 MPa (for 0 Ti) to 810 MPa (for 8 Ti). The difference in alloy strength between the two studies is mainly the result of larger γ'(L1$_2$) volume-fractions in the present Co-Ni-Al-W-Ti alloys, which may also be more resistant to shearing due to a higher concentration of (Al plus W plus Ti) of γ'(L1$_2$)-formers (18 vs. 12–17 at%), which may provide additional solid-solution strengthening and alter the APB and stacking fault energies.

5. Summary and conclusions

Multiple Co-10Ni-(9-x)Al-(9-x)W-2xTi alloys (x = 0, 1, 2, 3, 4) were cast and aged to obtain a γ(f.c.c.)-matrix plus γ'(L1$_2$)-precipitate microstructure. The effects of partially substituting Ti equally for both W and Al on the microstructural stability, phase compositions, and mechanical properties were studied utilizing scanning electron microscopy, compressive testing, Vickers microhardness testing, and differential thermal analyses. The following conclusions were reached:

- Substituting 1 at% Ti for 1 at% (W plus Al) reduces the mass density of Co-based superalloys by 0.10 g cm^{-3}, making them more competitive with advanced Ni-based superalloys.
- Replacing W and Al with Ti markedly increases the γ'(L1$_2$)-precipitate solvus temperature, from 1255 K (982 °C) in the 0 Ti alloy to 1410 K (1137 °C) in the 8 Ti alloy.
- Replacing W and Al with Ti strongly increases the peak flow-stress at high temperatures, from 575 MPa in the 0 Ti alloy to 810 MPa in the 8 Ti alloy between 700 and 900 °C.
- The γ'(L1$_2$)-precipitate structure is stable at 1273 K (1000 °C) for up to 1000 h in the Co-10Ni-(9-x)Al-(9-x)W-2xTi system.
  - The γ'(L1$_2$)-precipitate volume fraction does not decrease with increasing aging from 64 to 1000 h, indicating that the precipitates are most probably reasonably stable. The replacement of W and Al by Ti increases the volume fraction in alloys aged at 1273 K (1000 °C) for 64, 256, and 1000 h, ranging from 8.1 ± 2.7% to 49.9 ± 2.7%

- The replacement of W and Al by Ti increases the mean precipitate radius, < R > , ranging from 250 ± 63 nm to 722 ± 336 nm. The coarsening rate constants keeping the temporal exponent, p, constant at 3 are K = 3.6, 2.9, 9.1, and 16.6 × 10^{-26} m^3 s^{-1} for the 2, 4, 6, and 8 Ti alloys, which demonstrates that a reduction in the W concentration does result in an increase the coarsening rate, d < R(t) > /dt.
- Temporal exponents and coarsening rate constants were also calculated using a nonlinear multi-variate regression analysis. The inverse temporal exponents, 1/p, are 0.22, 0.24, 0.27, and 0.29, respectively, with corresponding coarsening rate constants calculated as 94.8 m$^{\frac{1}{0.22}}$ s^{-1}, 89.0 m$^{\frac{1}{0.24}}$ s^{-1}, 98.2 m$^{\frac{1}{0.27}}$ s^{-1}, and 104.2 m$^{\frac{1}{0.29}}$ s^{-1}.

- At 1273 K (1000 °C), the γ'(L1$_2$)-precipitates in Co-10Ni-6Al-6W-6Ti and Co-10Ni-5Al-5W-8Ti alloys coarsen with increasing aging time by the coagulation and coalescence mechanism, where the precipitates first coagulate, then grow and finally coalesce into one another to form micron-sized γ'(L1$_2$)-precipitates with irregular morphologies.
- Large W-rich μ(Co$_7$W$_6$)-type grain-boundary precipitates form on aging at 1273 K (1000 °C), measuring 1–3 µm in width, concurrent with precipitate-depleted zones, 2–20 µm wide. These μ(Co$_7$W$_6$)-type precipitates are present at grain boundaries, which could potentially serve as nucleation sites for unwanted phases that spread into the grain interior. Titanium segregates at grain boundaries and substitutes for W in the GB precipitates at up to 15.8 at% Ti.
- For each at% Ti replacing 1 at% W plus Al in the bulk alloy composition, the Al and W concentrations in the γ'(L1$_2$)-precipitates each decrease by 0.7 at%, while the Ti concentration increases by 1.3 at%.
- With increasing Ti and decreasing W and Al concentrations, the partitioning ratio of W increases from 1.23 ± 0.03 in the 2 Ti alloy to 1.50 ± 0.03 in the 8 Ti alloy, and conversely Al changes from a γ'(L1$_2$)- to a γ(f.c.c.)-former, with a decreasing partitioning ratio from 1.13 ± 0.07–0.94 ± 0.10.

Acknowledgements

References

[1] J. Sato, T. Omori, K. Oikawa, I. Ohnuma, R. Kainuma, K. Ishida, Cobalt-base high-temperature alloys, Science 312 (2006) 90–91.
[2] R.C. Reed, The Superalloys, Cambridge University Press, New York, 2006.
[3] C.T. Sims, N.S. Stoloff, W.C. Hagel, Superalloys II, John Wiley & Sons Inc, New York, 1987.
[4] M. Durand-Charre, The Microstructure of Superalloys, Gordon and Breach Science Publishers, Amsterdam, 1997.

[5] P. Caron, High γ′ solvus new generation Ni-based superalloys for single crystal turbine blade applications, Superalloys (2000) 737–746.

[6] T.M. Pollock, J. Dibbern, M. Tsunekane, J. Zhu, A. Suzuki, New Co-based γ-γ′ high-temperature alloys, JOM 62 (2010) 58–63.

[7] Y.M. Eggeler, M.S. Titus, A. Suzuki, T.M. Pollock, Creep deformation-induced antiphase boundaries in L1₂-containing single-crystal cobalt-base superalloys, Acta Mater. 77 (2014) 352–359.

[8] M.S. Titus, A. Suzuki, T.M. Pollock, Creep and directional coarsening in single crystals of new γ–γ′ cobalt-base alloys, Scr. Mater. 66 (2012) 574–577.

[9] M.S. Titus, A. Suzuki, T.M. Pollock, High temperature creep of new L1₂-containing cobalt-base superalloys, Superalloys 12 (2012) 823–831.

[10] K. Tanaka, M. Ooshima, N. Tsuno, A. Sato, H. Inui, Creep deformation of single crystals of new Co–Al–W-based alloys with fcc/L1₂ two-phase microstructures, Philos. Mag. 92 (2012) 4011–4027.

[11] L. Shi, J.J. Yu, C.Y. Cui, X.F. Sun, The creep deformation behavior of a single-crystal Co–Al–W-base superalloy at 900 °C, Mater. Sci. Eng. A 635 (2015) 50–58.

[12] L. Shi, J.J. Yu, C.Y. Cui, X.F. Sun, Temperature dependence of deformation behavior in a Co–Al–W-base single crystal superalloy, Mater. Sci. Eng. A 620 (2015) 36–43.

[13] L. Shi, J.J. Yu, C.Y. Cui, X.F. Sun, Effect of Ta additions on microstructure and mechanical properties of a single-crystal Co–Al–W-base alloy, Mater. Lett. 149 (2015) 58–61.

[14] F. Xue, H.J. Zhou, Q.Y. Shi, X.H. Chen, H. Chang, M.L. Wang, Q. Feng, Creep behavior in a γ′ strengthened Co–Al–W–Ta–Ti single-crystal alloy at 1000 °C, Scr. Mater. 97 (2015) 37–40.

[15] A. Bauer, S. Neumeier, F. Pyczak, M. Goken, Microstructure and creep strength of different γ/γ′-strengthened Co-base superalloy variants, Scr. Mater. 63 (2010) 1197–1200.

[16] A. Bauer, S. Neumeier, F. Pyczak, M. Göken, Creep strength and microstructure of polycrystalline γ′ – strengthened cobalt-base superalloys, Superalloys 12 (2012) 695–703.

[17] A. Bauer, S. Neumeier, F. Pyczak, R.F. Singer, M. Göken, Creep properties of different γ′-strengthened Co-base superalloys, Mater. Sci. Eng. A 550 (2012) 333–341.

[18] F. Pyczak, A. Bauer, M. Göken, S. Neumeier, U. Lorenz, M. Oehring, N. Schell, A. Schreyer, A. Stark, F. Symanzik, Plastic deformation mechanisms in a crept L1₂ hardened Co-base superalloy, Mater. Sci. Eng. A 571 (2013) 13–18.

[19] C.H. Zenk, S. Neumeier, H.J. Stone, M. Göken, Mechanical properties and lattice misfit of γ/γ′ strengthened Co-base superalloys in the Co–W–Al–Ti quaternary system, Intermetallics 55 (2014) 28–39.

[20] A. Suzuki, G.C. Denolf, T.M. Pollock, Flow stress anomalies in γ/γ′ two-phase Co–Al–W-base alloys, Scr. Mater. 56 (2007) 385–388.

[21] A. Suzuki, T.M. Pollock, High-temperature strength and deformation of γ/γ′ two-phase Co–Al–W-base alloys, Acta Mater. 56 (2008) 1288–1297.

[22] M.S. Titus, A. Mottura, G. Babu Viswanathan, A. Suzuki, M.J. Mills, T.M. Pollock, High resolution energy dispersive spectroscopy mapping of planar defects in L1₂-containing Co-base superalloys, Acta Mater. 89 (2015) 423–437.

[23] M.S. Titus, Y.M. Eggeler, A. Suzuki, T.M. Pollock, Creep-induced planar defects in L1₂-containing Co- and CoNi-base single-crystal superalloys, Acta Mater. 82 (2015) 530–539.

[24] N.L. Okamoto, T. Oohashi, H. Adachi, K. Kishida, H. Inui, P. Veyssiére, Plastic deformation of polycrystals of Co₃(Al,W) with the L1₂ structure, Philos. Mag. A 91 (2011) 3667–3684.

[25] S. Meher, H.-Y. Yan, S. Nag, D. Dye, R. Banerjee, Solute partitioning and site preference in γ/γ′ cobalt-base alloys, Scr. Mater. 67 (2012) 850–853.

[26] S. Meher, R. Banerjee, Partitioning and site occupancy of Ta and Mo in Co-base γ/γ′ alloys studied by atom probe tomography, Intermetallics 49 (2014) 138–142.

[27] P.J. Bocchini, E.A. Lass, K. Moon, M.E. Williams, C.E. Campbell, U.R. Kattner, D.C. Dunand, D.N. Seidman, Atom-probe tomographic study of γ/γ′ interfaces and compositions in an aged Co-Al-W superalloy, Scr. Mater. 68 (2012) 563–566.

[28] I. Povstugar, P.-P. Choi, S. Neumeier, A. Bauer, C.H. Zenk, M. Göken, D. Raabe, Elemental partitioning and mechanical properties of Ti- and Ta-containing Co–Al–W-base superalloys studied by atom probe tomography and nanoindentation, Acta Mater. 78 (2014) 78–85.

[29] T. Omori, K. Oikawa, J. Sato, I. Ohnuma, U.R. Kattner, R. Kainuma, K. Ishida, Partition behavior of alloying elements and phase transformation temperatures in Co-Al-W-base quaternary systems, Intermetallics 32 (2013) 274–283.

[30] H. Mughrabi, The importance of sign and magnitude of γ/γ′ lattice misfit in superalloys—with special reference to the new γ′-hardened cobalt-base superalloys, Acta Mater. 81 (2014) 21–29.

[31] S. Kobayashi, Y. Tsukamoto, T. Takasugi, H. Chinen, T. Omori, K. Ishida,

[32] S. Zaefferer, Determination of phase equilibria in the Co-rich Co–Al–W ternary system with a diffusion-couple technique, Intermetallics 17 (2009) 1085–1089.

[32] E.A. Lass, M.E. Williams, C.E. Campbell, K.-W. Moon, U.R. Kattner, γ′ phase stability and phase equilibrium in ternary Co-Al-W at 900 °C, J. Phase Equilib. Diffus. 35 (2014) 711–723.

[33] M. Ooshima, K. Tanaka, N.L. Okamoto, K. Kishida, H. Inui, Effects of quaternary alloying elements on the γ′ solvus temperature of Co–Al–W based alloys with fcc/L1₂ two-phase microstructures, J. Alloy. Compd. 508 (2010) 71–78.

[34] H.-Y. Yan, V.A. Vorontsov, D. Dye, Alloying effects in polycrystalline γ′ strengthened Co–Al–W base alloys, Intermetallics 48 (2014) 44–53.

[35] R.A. MacKay, T.P. Gabb, J.L. Smialek, M.V. Nathal, A. New, Approach of designing superalloys for low density, JOM 62 (2010) 48–54.

[36] T.M. Pollock, S. Tin, Nickel-based superalloys for advanced turbine engines: chemistry, Microstruct. Prop. JPP 22 (2006) 361–374.

[37] W.S. Walston, K.S. O'Hara, E.W. Ross, T.M. Pollock, W.H. Murphy, Rene N6: third generation single crystal superalloy, Superalloys (1996) 27–34.

[38] S. Kobayashi, Y. Tsukamoto, T. Takasugi, Phase equilibria in the Co-rich Co-Al-W-Ti quaternary system, Intermetallics 19 (2011) 1908–1912.

[39] K. Shinagawa, T. Omori, J. Sato, K. Oikawa, I. Ohnuma, R. Kainuma, K. Ishida, Phase equilibria and microstructure on γ′ phase in Co-Ni-Al-W system, Mater. Trans. JIM 49 (2008) 1474–1479.

[40] J.C. Russ, R.T. Dehoff, Practical Stereology, 2nd ed., Springer, New York, New York, 1986.

[41] C.K. Sudbrack, T.D. Ziebell, R.D. Noebe, D.N. Seidman, Effects of a tungsten addition on the morphological evolution, spatial correlations and temporal evolution of a model Ni–Al–Cr superalloy, Acta Mater. 56 (2008) 448–463.

[42] S.K. Makineni, B. Nithin, K. Chattopadhyay, Synthesis of a new tungsten-free γ–γ′ cobalt-based superalloy by tuning alloying additions, Acta Mater. 85 (2015) 85–94.

[43] S.K. Makineni, B. Nithin, K. Chattopadhyay, A new tungsten-free γ–γ′ Co–Al–Mo–Nb-based superalloy, Scr. Mater. 98 (2015) 36–39.

[44] Z. Mao, C.K. Sudbrack, K.E. Yoon, G. Martin, D.N. Seidman, The mechanism of morphogenesis in a phase-separating concentrated multicomponent alloy, Nat. Mater. 6 (2007) 210–216.

[45] I.M. Lifshitz, V.V. Slyozov, The kinetics of precipitation from supersaturated solid solutions, J. Phys. Chem. Solids 19 (1961) 35–50.

[46] C. Wagner, Theorie der Alterung von Niederschlagen durch Umlosen (Ostwald-Reifung), Z. Elektrochem. 65 (1961) 581–591.

[47] SigmaPlot. ⟨http://www.sigmaplot.com/products/sigmaplot/sigmaplot-details.php⟩: Systat Software.

[48] J.L. Murray, Co-Ti (Cobalt-Titanium), Binary Alloy Phase Diagrams, 2nd ed., ASM International, Materials Park, 1990.

[49] T. Grosdidier, A. Hazotte, A. Simon, Precipitation and dissolution processes in γ/γ′ single crystal nickel-based superalloys, Mater. Sci. Eng.: A 256 (1998) 183–196.

[50] T. Osada, Y. Gu, N. Nagashima, Y. Yuan, T. Yokokawa, H. Harada, New quantitative analysis of contributing factors to strength of disk superalloys, Superalloys (2012) 121–128.

[51] D. Tabor, The physical meaning of indentation and scratch hardness, Br. J. Appl. Phys. 7 (1956) 159–166.

[52] K. Shinagawa, T. Omori, K. Oikawa, R. Kainuma, K. Ishida, Ductility enhancement by boron addition in Co–Al–W high-temperature alloys, Scr. Mater. 61 (2009) 612–615.

[53] J.O. Singh, G.R. Purdy, Discontinuous precipitation in a dilute Co-3Ti-Nb ternary alloy, J. Mater. Sci. 22 (1987) 2918–2926.

[54] D.J. Sauza, P.J. Bocchini, D.C. Dunand, D.N. Seidman, Influence of ruthenium on microstructural evolution in a model CoAlW superalloy, Acta Mater. 117 (2016) 135–145.

[55] P.J. Bocchini, C.K. Sudbrack, R.D. Noebe, D.C. Dunand, D.N. Seidman, Microstructural and creep properties of boron- and zirconium-containing cobalt-based superalloys, Mater. Sci. Eng.: A 682 (2017) 260–269.

[56] F. Xue, H.J. Zhou, X.F. Ding, M.L. Wang, Q. Feng, Improved high temperature γ′ stability of Co–Al–W-base alloys containing Ti and Ta, Mater. Lett. 112 (2013) 215–218.

[57] B.H. Kear, J.M. Oblak, A.F. Giamei, Stacking faults in gamma prime Ni₃(Al,Ti) precipitation hardened nickel-base alloys, Metall. Mater. Trans. 1 (1970) 2477–2486.

[58] D.J. Crudden, A. Mottura, N. Warnken, B. Raeisinia, R.C. Reed, Modelling of the influence of alloy composition on flow stress in high-strength nickel-based superalloys, Acta Mater. 75 (2014) 356–370.